

## Electronic Supplementary Information (ESI)

# Water dispersible ligand-free rare earth fluoride nanoparticles: water transfer *versus* NaREF<sub>4</sub>-to-REF<sub>3</sub> phase transformation

Nan Liu,<sup>a</sup> Nicholas Gobeil,<sup>a</sup> Parrish Evers,<sup>a</sup> Isabel Gessner,<sup>a</sup> Emille M. Rodrigues,<sup>a</sup> and Eva Hemmer\*<sup>a,b</sup>

<sup>a</sup> Department of Chemistry and Biomolecular Sciences, University of Ottawa, 10 Marie-Curie Private, Ottawa (ON) K1N 6N5, Canada.

<sup>b</sup> Centre for Advanced Materials Research (CAMaR), University of Ottawa, Ottawa (ON) K1N 6N5, Canada.

\* Corresponding Author E-mail: ehemmer@uottawa.ca

## Table of Contents

1. Additional Experimental Details .....	2
2. Effect of Surface Chemistry and Particle Size .....	5
3. Influence of the pH on the Transformation of $\alpha$ -NaGdF <sub>4</sub> into GdF <sub>3</sub> .....	8
4. Influence of the Stirring Time on the Transformation of $\alpha$ -NaREF <sub>4</sub> into REF <sub>3</sub> .....	9
5. RE <sup>3+</sup> Ion Dependence – $\alpha$ -NaREF <sub>4</sub> as Starting NPs .....	10
6. Ho- and Lu-based NaREF <sub>4</sub> and REF <sub>3</sub> Structures – Phase/Morphology Assignment .....	12
7. RE <sup>3+</sup> Ion Dependence – $\beta$ -NaREF <sub>4</sub> as Starting NPs .....	15
8. Influence of Ln <sup>3+</sup> -Doping on the Formation of GdF <sub>3</sub> from $\alpha/\beta$ -NaGdF <sub>4</sub> .....	17
9. Steady State and Time-Resolved Spectroscopy of Ln <sup>3+</sup> -Doped $\alpha/\beta$ -NaGdF <sub>4</sub> and GdF <sub>3</sub> .....	19
10. References.....	23

## 1. Additional Experimental Details

**Table S1:** Overview of the experimental conditions used in the microwave-assisted synthesis of OA-capped  $\alpha/\beta$ -NaREF<sub>4</sub> NPs as well as the resulting average NP size ( $\pm$  standard deviation).

NaREF <sub>4</sub>	Ion Ratio (RE <sup>3+</sup> -to-Na <sup>+</sup> )	Ln <sup>3+</sup> Precursor Amount (mmol)	T <sub>1</sub> <sup>a</sup> (°C)	T <sub>2</sub> <sup>b</sup> (°C)	NaREF <sub>4</sub> Crystalline Phase	NaREF <sub>4</sub> Size (nm)
NaYF <sub>4</sub>	1:1	1.250	300	230	$\alpha$	8.6 $\pm$ 0.5
NaPrF <sub>4</sub>	1:1	1.250	300	230	$\alpha$	5.3 $\pm$ 0.5
	1:3	0.625	260	250	$\beta$	5.3 $\pm$ 0.6
NaNDF <sub>4</sub>	1:1	1.250	300	230	$\alpha$	4.8 $\pm$ 0.6
	1:3	0.625	260	250	$\beta$	6.5 $\pm$ 0.3
NaSmF <sub>4</sub>	1:1	1.250	300	230	$\alpha$	6.5 $\pm$ 0.6
	1:3	0.625	260	250	$\beta$	6.3 $\pm$ 0.2
NaEuF <sub>4</sub>	1:1	1.250	300	230	$\alpha$	7.8 $\pm$ 0.3
	1:3	0.625	260	250	$\beta$	6.4 $\pm$ 0.1
NaGdF <sub>4</sub> : Nd (10%)	1:1	1.250	300	230	$\alpha$	7.3 $\pm$ 0.4
	1:3	0.625	260	250	$\beta$	5.6 $\pm$ 0.2
NaGdF <sub>4</sub> : Eu (10%)	1:1	1.250	300	230	$\alpha$	8.1 $\pm$ 0.4
NaGdF <sub>4</sub>	1:1	1.250	300	230	$\alpha$	7.4 $\pm$ 0.4
	1:2	1.250	260	250	$\beta$	5.9 $\pm$ 0.5
NaGdF <sub>4</sub> : Tb (10%)	1:1	1.250	300	230	$\alpha$	7.2 $\pm$ 0.5
NaGdF <sub>4</sub> : Er/Yb (2%/20%)	1:1	1.250	300	230	$\alpha$	8.4 $\pm$ 0.3
	1:1 <sup>c</sup>	0.625	-	230	$\alpha$	11.7 $\pm$ 0.9
	1:3	0.625	260	250	$\beta$	6.5 $\pm$ 0.4
NaTbF <sub>4</sub>	1:3 <sup>c</sup>	0.625	-	230	$\beta$	7.4 $\pm$ 0.5
	1:1	1.250	300	230	$\alpha$	6.3 $\pm$ 0.8
NaDyF <sub>4</sub>	1:3	0.625	260	250	$\beta$	6.5 $\pm$ 0.6
	1:1	1.250	300	230	$\alpha$	5.2 $\pm$ 0.8
NaHoF <sub>4</sub>	1:3	0.625	260	250	$\beta$	6.8 $\pm$ 0.2
	1:1	1.250	300	230	$\alpha$	5.6 $\pm$ 0.8
NaErF <sub>4</sub>	1:1	1.250	300	230	$\alpha$	6.3 $\pm$ 1.0
NaYbF <sub>4</sub>	1:1	1.250	300	230	$\alpha$	7.6 $\pm$ 1.0
NaLuF <sub>4</sub>	1:1	1.250	300	230	$\alpha$	6.3 $\pm$ 1.0

<sup>a</sup> Holding time at T<sub>1</sub> = 1 s

<sup>b</sup> Reaction time at T<sub>2</sub> = 10 min

<sup>c</sup> Reaction conditions for growing an undoped NaGdF<sub>4</sub> shell

**Table S2:** Overview of the experimental conditions used for the evaluation of the pH dependence of the ligand removal for  $\alpha$ -NaGdF<sub>4</sub> NPs and size of the resulting GdF<sub>3</sub> NPs.

pH	Stirring Time (h)	Transfer into Aqueous Phase	GdF <sub>3</sub> Formation	GdF <sub>3</sub> Crystalline Phase	GdF <sub>3</sub> NP Diameter (nm)	GdF <sub>3</sub> NP Thickness (nm)
1		yes	yes	hexagonal	<sup>a</sup>	-
1.5		yes	yes	hexagonal	174 ± 45	-
2	20	yes	yes	hexagonal	147 ± 34	-
2.5		yes	yes	hexagonal	171 ± 39	45 ± 13
3		no	no	no	<sup>b</sup>	-

<sup>a</sup> Due to the non-defined morphology of the obtained NPs, it was not possible to obtain any size distribution.

<sup>b</sup> At this pH, no product was found in the aqueous phase, yet, the OA-capped  $\alpha$ -NaGdF<sub>4</sub> NPs could be easily recovered from the organic phase after precipitation with ethanol.

**Table S3:** Overview of the experimental conditions used for the evaluation of the effect of stirring time on the ligand removal procedure for  $\alpha$ -NaGdF<sub>4</sub> NPs (pH 1.5) and size of the resulting GdF<sub>3</sub> NPs.

NaREF <sub>4</sub>	NaGdF <sub>4</sub> Crystalline Phase	Stirring Time (h)	GdF <sub>3</sub> NP Diameter (nm)
		1	162 ± 47
		4	180 ± 44
NaGdF <sub>4</sub>	$\alpha$	8	160 ± 53
		20	174 ± 45

**Table S4:** Overview of the experimental conditions used for the evaluation of the RE<sup>3+</sup> ion dependence on the phase transformation into RE<sub>3</sub>F upon ligand removal (pH 1.5). The table also summarizes whether or not a phase transformation took place and provides the average size ( $\pm$  standard deviation) of the obtained ligand-free (LF) particles.

<b>NaREF<sub>4</sub></b>	<b>NaREF<sub>4</sub> Crystalline Phase</b>	<b>Stirring Time (h)</b>	<b>REF<sub>3</sub> Formation</b>	<b>LF-NP Size (nm)</b>
<b>NaYF<sub>4</sub></b>	$\alpha$	4	no	8.5 $\pm$ 0.6
<b>NaPrF<sub>4</sub></b>	$\alpha$	4	yes	22.0 $\pm$ 3.1
	$\beta$	20	yes	29.8 $\pm$ 8.0
<b>NaNdF<sub>4</sub></b>	$\alpha$	4	yes	41.7 $\pm$ 9.8
	$\beta$	20	yes	239 $\pm$ 79
<b>NaSmF<sub>4</sub></b>	$\alpha$	4	yes	43.5 $\pm$ 13.0
	$\beta$	20	yes	236 $\pm$ 125
<b>NaEuF<sub>4</sub></b>	$\alpha$	4	yes	83.6 $\pm$ 21.0
	$\beta$	20	no	7.2 $\pm$ 0.2
<b>NaGdF<sub>4</sub>: Nd (10%)</b>	$\alpha$	20	yes	86.1 $\pm$ 21.5
	$\beta$	20	no	5.5 $\pm$ 0.3
<b>NaGdF<sub>4</sub>: Eu (10%)</b>	$\alpha$	20	yes	144 $\pm$ 38
<b>NaGdF<sub>4</sub></b>	$\alpha$	4	yes	180 $\pm$ 44
	$\beta$	20	no	5.9 $\pm$ 0.3
<b>NaGdF<sub>4</sub>: Tb (10%)</b>	$\alpha$	20	yes	185 $\pm$ 43
<b>NaGdF<sub>4</sub>: Er/Yb (2%/20%)</b>	$\alpha$	20	yes	164 $\pm$ 22 <sup>a</sup>
	$\beta$	20	no	6.2 $\pm$ 0.2
<b>NaTbF<sub>4</sub></b>	$\alpha$	4	yes	391 $\pm$ 101 <sup>b</sup>
	$\beta$	20	no	6.1 $\pm$ 0.5
<b>NaDyF<sub>4</sub></b>	$\alpha$	4	no	5.6 $\pm$ 0.9
	$\beta$	20	no	6.6 $\pm$ 0.3
<b>NaHoF<sub>4</sub></b>	$\alpha$	4	partially	16.7 $\pm$ 5.2 <sup>c</sup>
<b>NaErF<sub>4</sub></b>	$\alpha$	4	no	6.6 $\pm$ 1.0
<b>NaYbF<sub>4</sub></b>	$\alpha$	4	no	7.2 $\pm$ 1.0
<b>NaLuF<sub>4</sub></b>	$\alpha$	4	partially	6.8 $\pm$ 1.2 <sup>d</sup>

<sup>a</sup> Length of the prismatic particles; for thickness and width, see Figure S14.<sup>b</sup> Diameter of the plates; for thickness, see Figure S8.<sup>c</sup> Length of the RE<sub>3</sub>F rods; for thickness of the rods and size of the non-transformed NaREF<sub>4</sub> NPs, see Figure S8.<sup>d</sup> Diameter of the small NPs, for size of the ribbon-like structures, see Figure S8 and S9.

## 2. Effect of Surface Chemistry and Particle Size

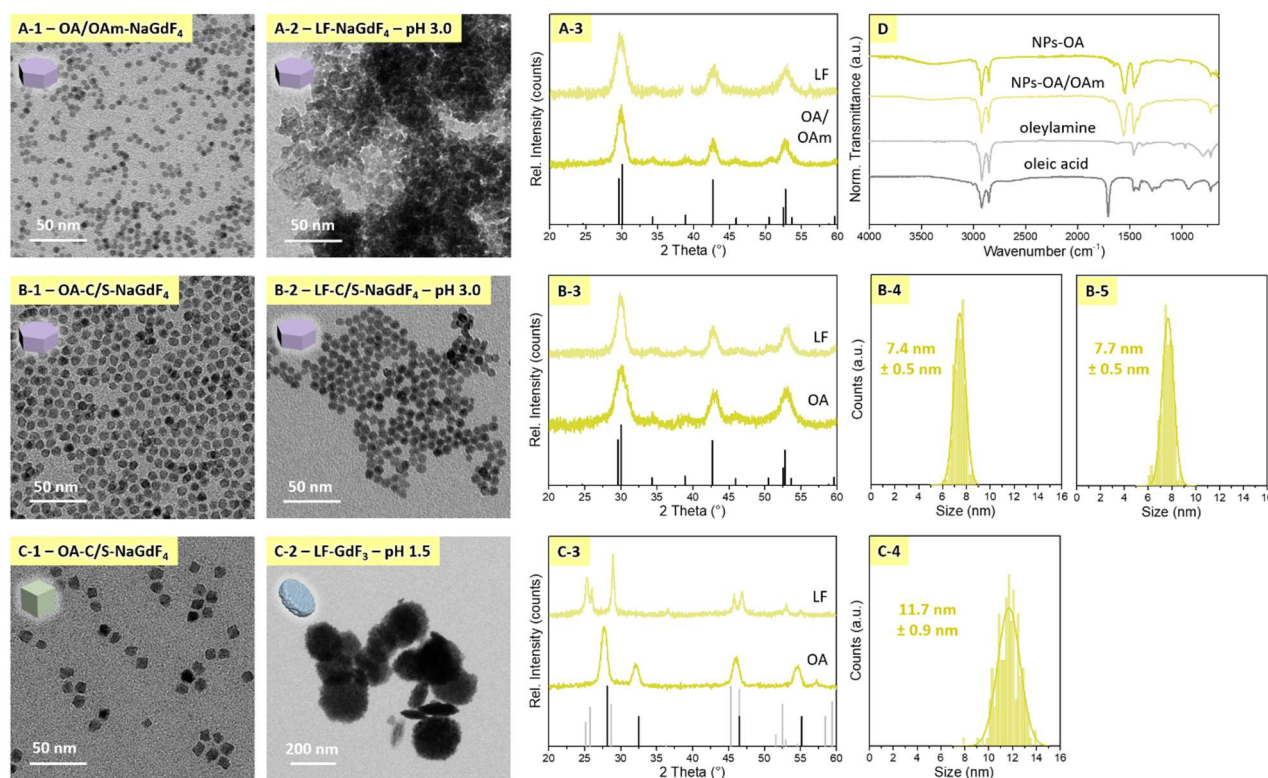


**Figure S1:** Effect of (A) the NaREF<sub>4</sub> crystalline phase on the pH necessary for ligand removal, (B) surface chemistry on ligand removal, and (C) particle size on phase transformation upon ligand removal. (A-1/2) TEM images of  $\beta$ -NaGdF<sub>4</sub> NPs synthesized using OA and OAm before and after ligand removal at pH 3 (20 h) reveal the poor quality of LF-NPs obtained under these conditions. XRD patterns of both samples are shown in (A-3). Reflections at 39° due to NaF (a possible by-product of NP synthesis)<sup>1</sup> were removed for clarity. Size and size distribution of (A-1) are given in Figure 1A-4. (B-1/2) TEM images of core/shell  $\beta$ -NaGdF<sub>4</sub>:Er<sup>3+</sup>,Yb<sup>3+</sup>/NaGdF<sub>4</sub> NPs (only OA was used during shell growth) before and after ligand removal at pH 3 (20 h) demonstrate the successful transfer of the NPs into the aqueous phase. XRD patterns of both samples are shown in (B-3). Size and size distribution are given in (B-4/5). (C-1/2) TEM images of larger core/shell  $\alpha$ -NaGdF<sub>4</sub>:Er<sup>3+</sup>,Yb<sup>3+</sup>/NaGdF<sub>4</sub> NPs before and after ligand removal at pH 1.5 (4 h) indicate phase transformation into hexagonal GdF<sub>3</sub> (see C-3 for XRD patterns) despite the larger particle size (no OAm was used for shell growth). (C-4) Size and size distribution of (C-1). (D) Representative FTIR spectra recorded of NaGdF<sub>4</sub> NPs grown in the presence (NPs-OA/OAm) and absence (NPs-OA) of OAm, respectively. Spectra obtained of pure oleic acid and oleylamine used in the synthesis are also shown. References:  $\beta$ -NaGdF<sub>4</sub>, PDF card [01-080-8787] (black line in A/B-3);  $\alpha$ -NaGdF<sub>4</sub>, PDF card [00-027-0697] (black line in C-3); hexagonal EuF<sub>3</sub>, PDF card [00-032-0373] (light grey line in C-3).

**Assessment of pH for successful ligand removal.** As discussed in the main manuscript, a pH < 3 was deemed necessary to transfer OA/OAm-capped  $\alpha$ -NaGdF<sub>4</sub> NPs from the organic into the aqueous phase. Conversely, in case of  $\beta$ -NaGdF<sub>4</sub> NPs, the synthesis of which also included oleic acid and oleylamine as solvent and capping agent, ligand-free  $\beta$ -NaGdF<sub>4</sub> NPs could be transferred at pH 3 (samples shown in Figure S1A-1 are the same batch of NPs as those used for ligand removal at pH 1.5, Figure 1A). The crystalline phase of the LF-NPs was confirmed by XRD analysis (Figure S1A-3). Yet, as evident from Figure S1A-2, the LF-NPs suffered from severe aggregation and lost their crisp spherical morphology. Based on these findings, a pH value of 3 was deemed unsuitable for the successful preparation of ligand-free  $\beta$ -NaGdF<sub>4</sub> NPs.

**Effect of surface chemistry.** The use of both oleylamine and oleic acid during NP synthesis is expected to result in NPs capped with OA and OAm groups. FTIR spectra shown in Figure S1D confirmed the presence of OA. The peaks at 2926 cm<sup>-1</sup> and 2850 cm<sup>-1</sup> can be assigned to the asymmetric and symmetric stretching of -CH<sub>2</sub> groups

while the peaks at  $1550\text{ cm}^{-1}$  and  $1460\text{ cm}^{-1}$  originate from the asymmetric ( $\delta_{as}$ ) and symmetric ( $\delta_s$ )  $-\text{COO}^-$  stretching.<sup>2</sup> The presence of OAm could not be unambiguously confirmed by FTIR spectroscopy given the overlap of the spectral features for both compounds, neither can its presence be ruled out.

In order to investigate the influence of surface chemistry, *i.e.* the presence of OAm on the NP surface, a batch of  $\beta\text{-NaGdF}_4$  NPs of comparable size was synthesized without oleylamine. As the microwave-assisted approach requires the presence of oleylamine as a surfactant in addition to oleic acid to yield NPs of homogeneous morphology, it was not possible to simply omit oleylamine during the reaction. Conveniently, no oleylamine is used for the microwave-assisted growth of a thin shell onto the NPs. Hence, first, OA/OAm-capped NPs were synthesized (in this case:  $\beta\text{-NaGdF}_4\text{:Er}^{3+},\text{Yb}^{3+}$ ), followed by a washing step to remove any oleylamine from the reaction mixture prior to subsequent shell growth (pure  $\text{NaGdF}_4$ ) using solely oleic acid in addition to octadecene as solvent (see Experimental Section in the main manuscript for details). This strategy allowed to obtain  $\beta\text{-NaGdF}_4\text{:Er}^{3+},\text{Yb}^{3+}/\text{NaGdF}_4$  NPs, most likely being only capped with OA (Figure S1: TEM – B-1; XRD – B-3; Size – B-4, FTIR – D). The thickness of the shell was estimated to be 0.7 nm, based on TEM images recorded of the core-only NPs before the addition of the shell precursor (data not shown).

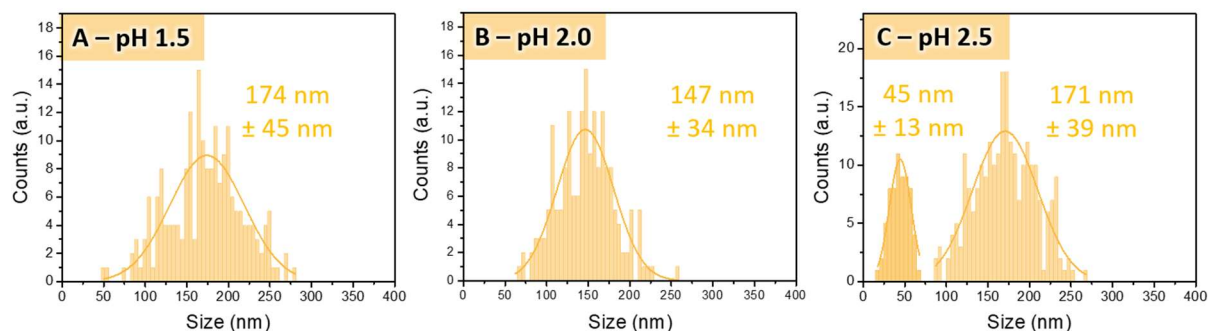
Obtained OA-capped core/shell NPs were treated with a HCl solution at pH 3 for 20 h to assess the ligand removal. The resulting NPs were transferred successfully to the aqueous phase, without any phase transformation (Figure S1B). It should be noted that this was the only sample that underwent an organic-to-aqueous phase transfer retaining morphology at pH 3. These observations indicate the importance of surface chemistry for ligand removal, *i.e.* the presence of OAm groups requiring lower pH. In light of this, the use of pH 3-4 for ligand removal reported in the literature may be related to the fact that many of these studies revolve around NPs that – based on their synthesis method – are only OA-capped.<sup>3-6</sup> In addition, it is notable that successful ligand removal at pH 4 is typically achieved on  $\text{NaREF}_4$  NPs crystallized in the hexagonal phase and of larger size.<sup>5,6</sup> Consequently, it is hypothesized that both surface chemistry and particle size (the latter being briefly addressed in the following paragraph) have an influence on conditions required for ligand removal. Further investigation of a broad range of NPs exhibiting various sizes and surface chemistries may provide clarification, yet are beyond the scope of this study.

Besides the potential influence of the ligand on pH requirements, phase transformation itself is thought not to be governed (neither prevented nor fostered) by the presence of OA/OAm ligands. In case of stable NPs, upon re-protonation, oleic acid migrates into the organic phase, while ligand-free NPs are dispersed in the (still acidic) aqueous phase. Even under prolonged stirring (*e.g.*, 20 h), these ligand-free NPs did not undergo phase transformation, despite lack of any protecting OA/OAm ligands on their surface. In case of instable NPs, the phase transformation takes place in the aqueous phase of the bi-phasic mixture used for ligand removal: The dissolution and re-precipitation processes are ruled by the relative thermodynamic stability of each  $\text{NaREF}_4$  and  $\text{REF}_3$ , which in turn, depends on the equilibrium of the solvated ions and the precipitated NPs in the aqueous phase. Hence, the here observed (in)stability of  $\text{NaREF}_4$  NPs under acidic conditions is rather due to the intrinsic materials properties than due to the synthesis-related OA/OAm ligands.

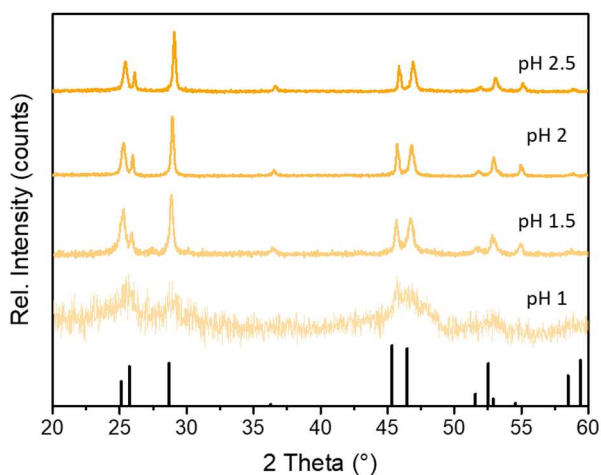
**Size effect.** In addition, it was investigated whether larger NP size may prevent phase transformation from  $\alpha\text{-NaGdF}_4$  into  $\text{GdF}_3$  upon treatment at pH 1.5 (4 h). Given that surface grows significantly over volume upon decreasing particle size, the larger surface of small NPs – as used in this study – may enhance the interaction with  $\text{H}^+$  ions in the acidic solution, thus, challenging chemical stability. As the microwave-assisted approach generally provides access to small NPs at the sub-10 nm realm, the core/shell strategy was applied to obtain larger NPs, namely  $\alpha\text{-NaGdF}_4\text{:Er}^{3+},\text{Yb}^{3+}/\text{NaGdF}_4$  NPs of almost 12 nm in size (Figure 1S C). Yet, TEM and XRD analysis revealed that phase transformation into  $\text{GdF}_3$  took place. Hence, while larger sizes may endow the NPs with chemical stability, size effects at the size scale accessible by our microwave-assisted approach can

be ruled out. Finally, it should be mentioned that the obtained ligand-free  $\text{GdF}_3$  NPs exhibited a hexagonal crystalline phase. This is in contrast to  $\text{GdF}_3:\text{Er}^{3+},\text{Yb}^{3+}$  obtained from  $\alpha\text{-NaGdF}_4:\text{Er}^{3+},\text{Yb}^{3+}$  core-only NPs (Figure 7), which crystallized in the orthorhombic phase. The presence of the undoped shell, *i.e.*  $\alpha\text{-NaGdF}_4$ , may explain this behaviour as pure  $\alpha\text{-NaGdF}_4$  was shown to transform into hexagonal  $\text{GdF}_3$ .

### 3. Influence of the pH on the Transformation of $\alpha$ -NaGdF<sub>4</sub> into GdF<sub>3</sub>

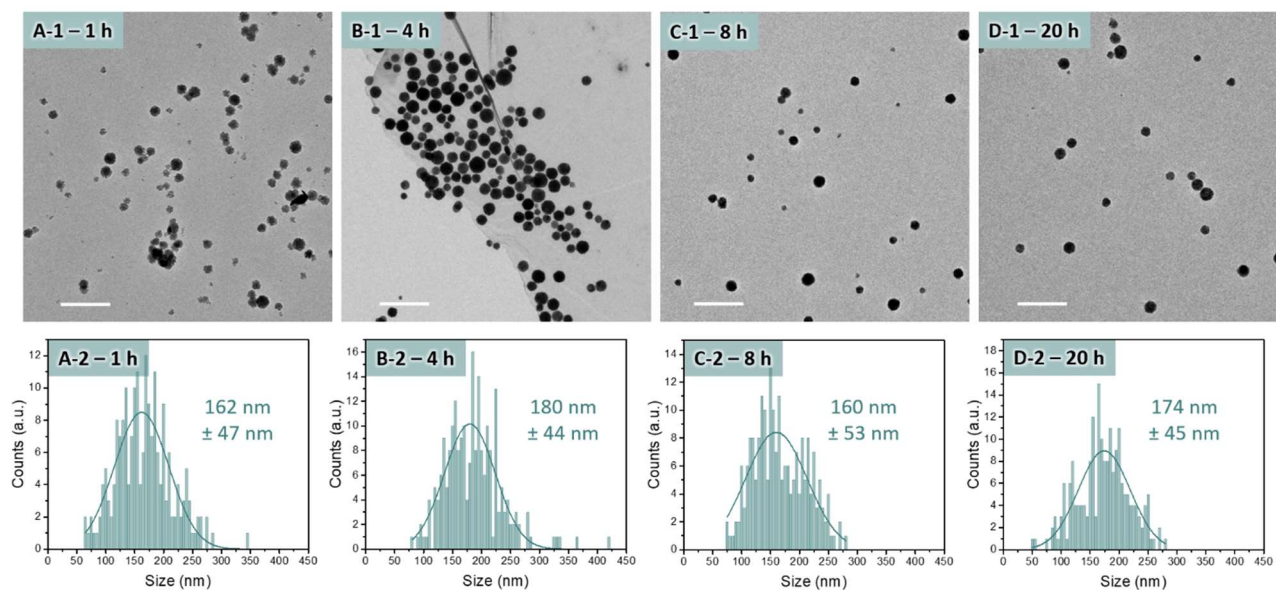


**Figure S2:** Average sizes and size distributions of particles obtained upon treatment of  $\alpha$ -NaGdF<sub>4</sub> NPs for 20 h at (A) pH 1.5, (B) pH 2.0, and (C) pH 2.5, respectively. (C) In addition to the diameter, the average thickness of the plate-like structures is given as determined from plates that self-arranged perpendicular to the TEM grid. Similar dimensions were observed for the other GdF<sub>3</sub> structures.

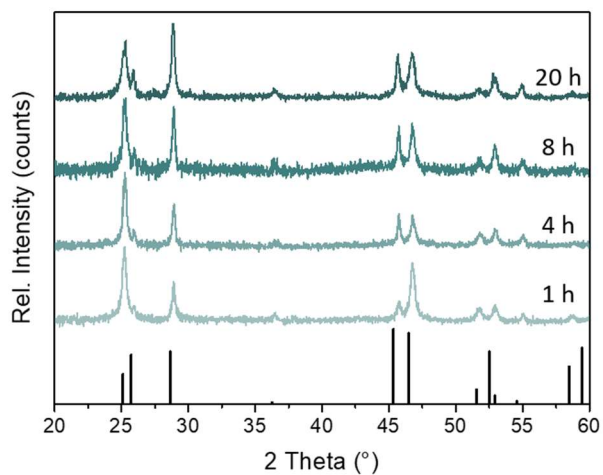


**Figure S3:** XRD patterns of particles obtained upon treatment of  $\alpha$ -NaGdF<sub>4</sub> NPs for 20 h at pH 1, 1.5, 2, and 2.5, respectively. Reference: hexagonal EuF<sub>3</sub>, PDF card [00-032-0373].

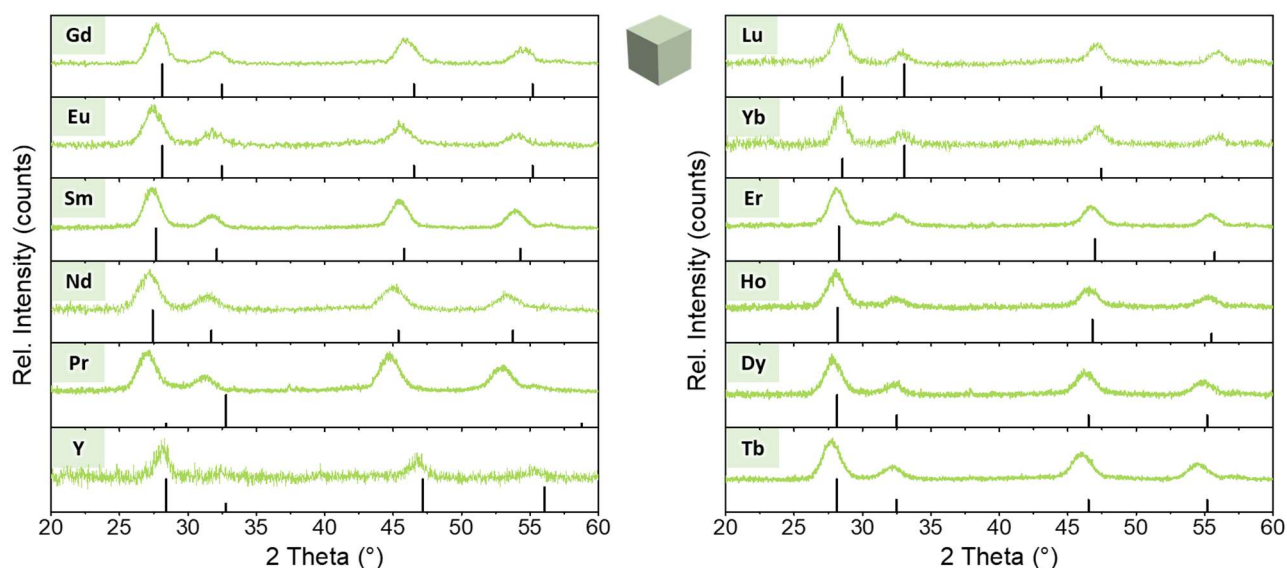
#### 4. Influence of the Stirring Time on the Transformation of $\alpha$ -NaREF<sub>4</sub> into REF<sub>3</sub>



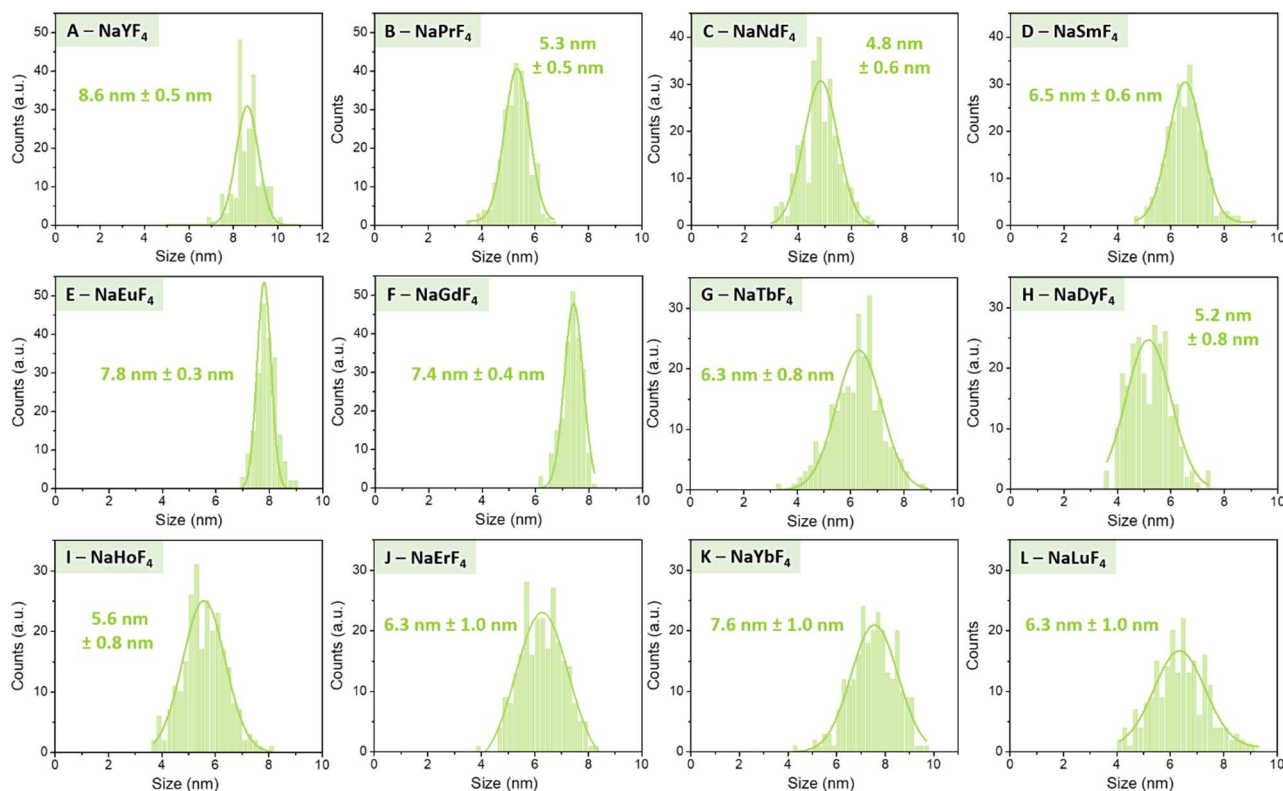
**Figure S4:** (1) Lower magnification TEM images and (2) size distributions of hexagonal GdF<sub>3</sub> particles obtained by stirring of  $\alpha$ -NaGdF<sub>4</sub> NPs at pH 1.5 for (A) 1 h, (B) 4 h, (C) 8 h, and (D) 20 h, respectively. Scale bars: 1  $\mu$ m.



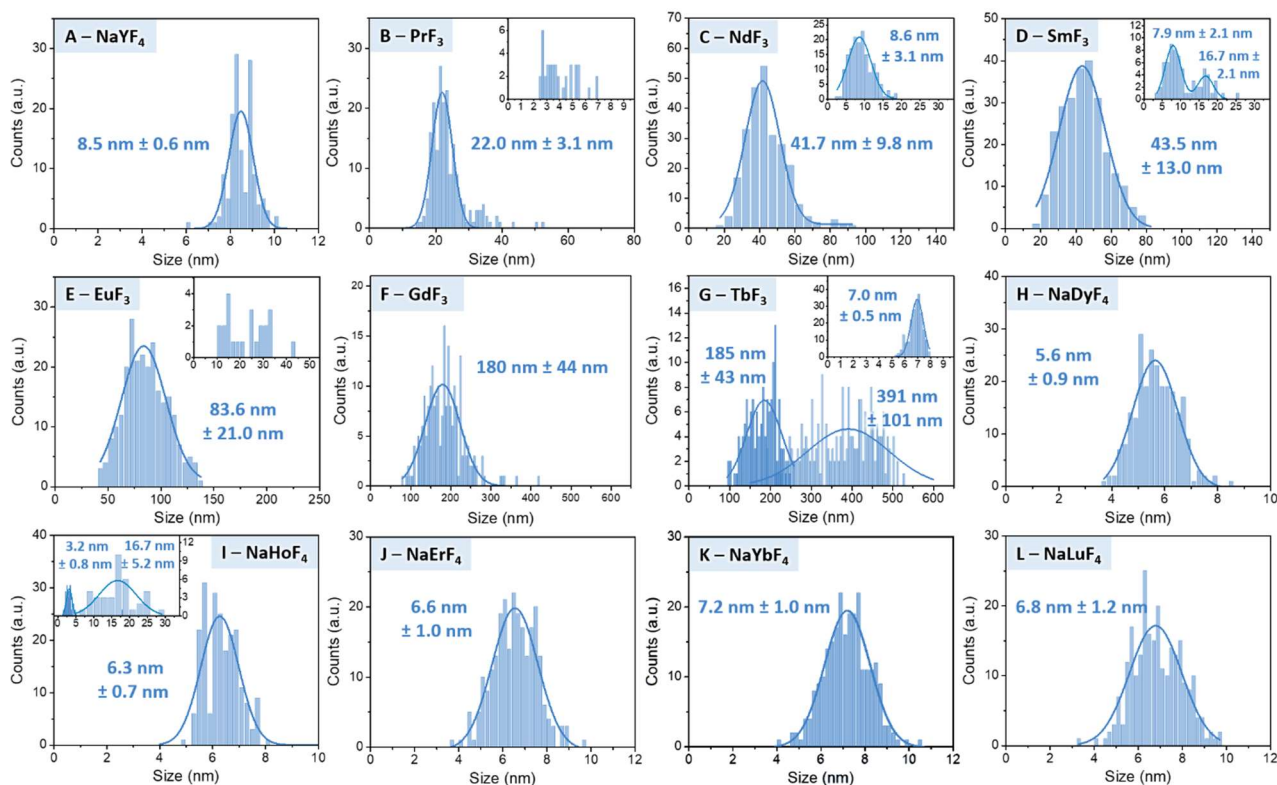
**Figure S5:** XRD patterns revealing hexagonal GdF<sub>3</sub> as the sole crystalline phase upon treatment of  $\alpha$ -NaGdF<sub>4</sub> NPs at pH 1.5 for 1, 4, 8, and 20 h, respectively. Reference: hexagonal EuF<sub>3</sub>, PDF card [00-032-0373].

5. RE<sup>3+</sup> Ion Dependence –  $\alpha$ -NaREF<sub>4</sub> as Starting NPs

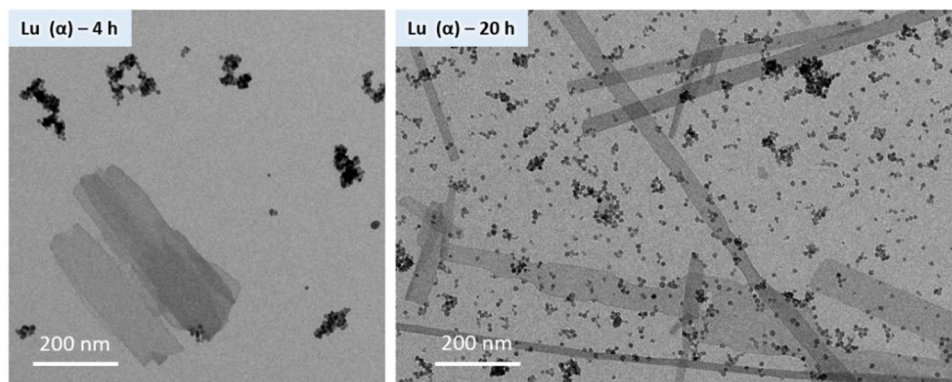
**Figure S6:** XRD patterns of  $\alpha$ -NaREF<sub>4</sub> NPs obtained by microwave-assisted thermal decomposition. RE refers to the rare earth ions studied as labelled for each pattern. References:  $\alpha$ -NaYF<sub>4</sub>, PDF card [00-006-0342];  $\alpha$ -NaPrF<sub>4</sub>, PDF card [00-022-1393];  $\alpha$ -NaNdF<sub>4</sub>, PDF card [00-028-1114];  $\alpha$ -NaSmF<sub>4</sub>, PDF card [00-027-0778];  $\alpha$ -NaGdF<sub>4</sub>, PDF card [00-027-0697] (this card was also used for RE = Eu, Tb, Dy);  $\alpha$ -NaHoF<sub>4</sub>, PDF card [01-077-2040];  $\alpha$ -NaErF<sub>4</sub>, PDF card [01-077-2041];  $\alpha$ -NaYbF<sub>4</sub>, PDF card [01-077-2043] (this card was also used for RE = Lu).



**Figure S7:** Average sizes and size distributions of the OA-capped  $\alpha$ -NaREF<sub>4</sub> NPs shown in Figure 4 (A1 to L1) used for ligand removal (pH 1.5, 4 h).



**Figure S8:** Average sizes and size distributions of the ligand-free NPs shown in Figure 4 (A2 to L2) obtained by treatment of the OA-capped  $\alpha$ -NaREF<sub>4</sub> NPs at pH 1.5 for 4 h. The insets in B to E provide an estimated value for the thickness of the obtained plates. Dimensions given in G correspond to the length, width and thickness of the TbF<sub>3</sub> bundle-like structures. The inset in I shows the length and width of the nanorods ascribed to HoF<sub>3</sub> as minor, secondary phase.

6. Ho- and Lu-based NaREF<sub>4</sub> and REF<sub>3</sub> Structures – Phase/Morphology Assignment

**Figure S9:** TEM image of ligand-free NPs and ribbon-like structures obtained upon stirring OA-capped  $\alpha$ -NaLuF<sub>4</sub> NPs at pH 1.5 for 4 and 20 h, respectively.

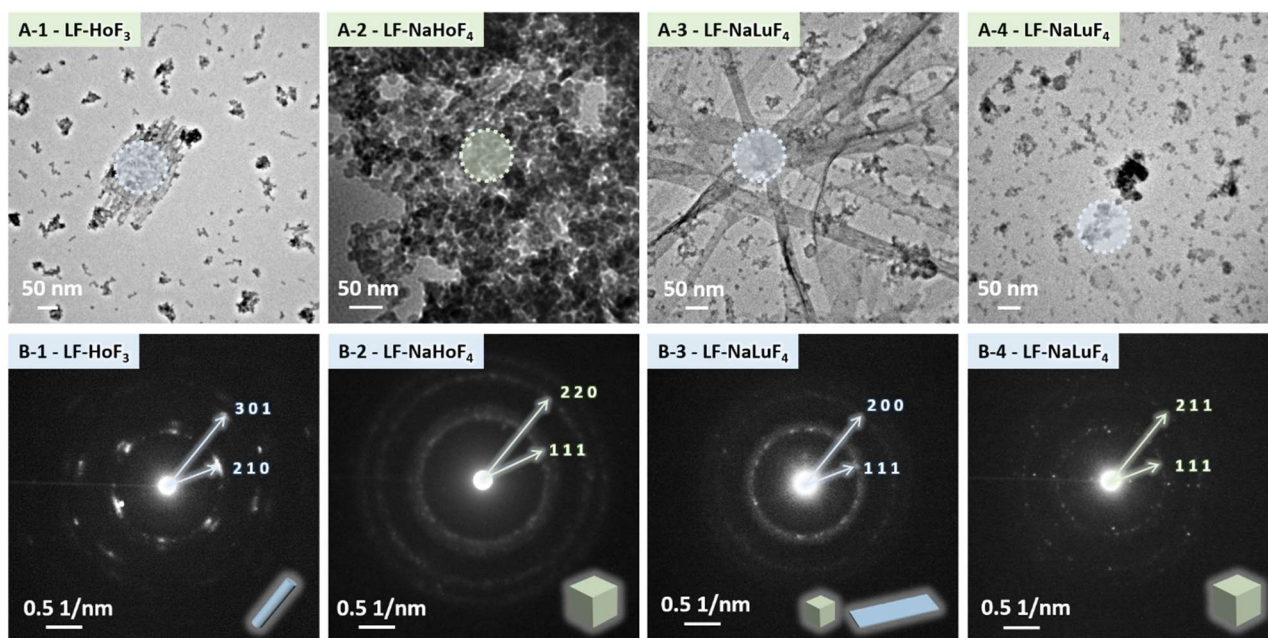


**Figure S10:** (A) TEM images showing the highlighted areas from which the selected area electron diffraction (SAED) patterns shown in (B) were obtained. (1) LF-HoF<sub>3</sub> structures of rod-like morphology, (2) LF-NaHoF<sub>4</sub> NPs, (3) LF-LuF<sub>3</sub> band-like structures; (4) LF-NaLuF<sub>4</sub> NPs.

As discussed in the main text, both the XRD patterns shown in Figure 5 and the TEM images shown in Figure 4 indicated the presence of a minor fraction of orthorhombic HoF<sub>3</sub> and LuF<sub>3</sub> for the LF-NaHoF<sub>4</sub> and LF-NaLuF<sub>4</sub> samples, respectively. To further validate the assignment of the crystalline phases to specific morphologies, selected area electron diffraction (SAED) analysis was performed in the selected regions highlighted in Figure S10. The respective areas in (A-1) and (A-3) contain primarily rod-like (Ho) or ribbon-like (Lu) structures, whereas the areas shown in (A-2, Ho) and (A-4, Lu) contain spherical NPs, which allowed for an assessment of each morphology.

The interplanar distances ( $d_{SAED}$ ) were calculated based on the camera length calibration with a standard Au sample (Au foil,  $d_{Au} = 0.204 \text{ \AA}$  for the first ring) using a derivation of Bragg's equation:

$$d = \frac{\lambda L}{R} \quad (\text{Eq. 1})$$

where,

$d$  = interplanar distance

$\lambda$  = wavelength of the diffracted electrons

$L$  = camera length

and by adopting the ratio between the radius of the first ring of the SAED image of the Au standard and that of the sample:

$$\frac{d_{sample}}{d_{Au}} = \frac{R_{Au}}{R_{sample}} \text{ (Eq. 2)}$$

where,

$R_{Au}$  = radius of the SAED ring of the Au standard

$R_{sample}$  = radius of the SAED ring for the sample

$d_{Au}$  = interplanar distance of the Au foil for the corresponding ring

For comparison, the  $d_{XRD}$  distances obtained for the main XRD reflections at the  $2\theta$  range from 25 to 50 ° for Ho- and Lu-based patterns shown at Figure 5 were calculated by direct application of Bragg equation:

$$n\lambda = 2d_{XRD}\sin\theta \text{ (Eq. 3)}$$

where,

$n = 1$  (first order diffraction)

$\lambda = 1.5406 \text{ \AA}$

$\sin\theta \cong \theta$ , for small  $\theta$

**Table S5:** Comparison between the values of the interplanar distances ( $d$ ) calculated from Scherrer equation using the main reflections in the recorded XRD patterns shown in Figure 5, those obtained from the first and second rings of the SAED patterns shown in Figure S10, and the standard values from the PDF cards for the Ho- and Lu-based samples.

Sample	$2\theta$ (°)	$d_{XRD}$ (Å)	$d_{SAED}$ (Å)	$d_{PDF}$ (Å)	$h k l$	Crystalline Phase	PDF #
LF-NaHoF <sub>4</sub>	27.94	3.19	3.15	3.17	1 1 1	$\alpha$ -NaHoF <sub>4</sub>	01-077-2040
	30.40	2.94	3.02	2.90	2 1 0	HoF <sub>3</sub>	00-023-0284
	32.36 *	2.77	-	2.74	2 0 0	$\alpha$ -NaHoF <sub>4</sub>	01-077-2040
	46.42 †	1.95	1.91	1.94	2 2 0	$\alpha$ -NaHoF <sub>4</sub>	01-077-2040
1.90			1.94	1 3 1	HoF <sub>3</sub>	00-023-0284	
LF-NaLuF <sub>4</sub>	25.74 *	3.46	-	3.38	0 2 0	LuF <sub>3</sub>	00-032-0612
	28.34	3.15	3.09	3.19	1 1 1	LuF <sub>3</sub>	00-032-0612
			3.10	3.13	1 1 1	$\alpha$ -NaLuF <sub>4</sub>	01-077-2043
	32.80 *	2.73	-	2.70	2 0 0	$\alpha$ -NaLuF <sub>4</sub>	01-077-2043
	47.20 †	1.92	1.88	1.91	2 2 0	$\alpha$ -NaLuF <sub>4</sub>	01-077-2043
1.90			1.91	1 3 1	LuF <sub>3</sub>	00-032-0612	

\* These diffractions were present in the XRD patterns but were not observed by SAED analysis.

† These diffractions were present both in the XRD patterns and SAED analysis, however, they are common to both crystalline phases and, therefore, are not suitable to distinguish between the  $\alpha$ -NaREF<sub>4</sub> and REF<sub>3</sub> phases.

The interplanar distances obtained from the SAED patterns for the small spherical NPs of the Ho-based sample (Figure S10, A/B-2) reveal an interplanar distance of 3.15 Å attributed to the  $\alpha$ -NaHoF<sub>4</sub> (1 1 1) planes (Table S5, highlighted in green). These findings confirm that  $\alpha$ -NaHoF<sub>4</sub> partially resisted to the phase transformation into HoF<sub>3</sub>. Further, the size of the small spherical LF-NPs (Figure S8-I) was very close to the size of the used OA-capped NPs (Figure S7-I), which corroborates the suggested phase/morphology assignment. SAED patterns of the rod-like structures of the same sample (Figure S10, A/B-1) correspond to an interplanar distance of 3.02 Å, which can be assigned to the (2 1 0) planes of the orthorhombic HoF<sub>3</sub> crystalline structure (Table S5, highlighted in green). Overall, these observations show that a phase transformation started to take place in this sample, with a clear morphological difference between the two phases as confirmed by SAED and TEM analysis.

For the Lu-based samples, however, both the SAED patterns of the small spherical NPs (Figure S10, A/B-4) and of the ribbon-like structures (Figure S10, A/B-3) showed very similar interplanar distances of 3.09 and 3.10 Å, respectively, which can be attributed to the (1 1 1) planes from either the  $\alpha$ -NaLuF<sub>4</sub> or the orthorhombic LuF<sub>3</sub> crystalline phases (Table S5). Therefore, an unambiguous attribution of the planes was not possible, as the interplanar distances found from the SAED patterns and the respective standards are too close to both the  $\alpha$ -NaLuF<sub>4</sub> and orthorhombic LuF<sub>3</sub> reflections (Table S5). This observation is in line with the XRD patterns shown in Figure 5, where the presence of the cubic-phase NaLuF<sub>4</sub> is clear but a phase mix with the orthorhombic LuF<sub>3</sub> cannot be ruled out. Nevertheless, having been able to clearly ascribe a crystalline phase to each of the morphologies in the Ho-based samples, we propose a similar case for the Lu-based samples. As such, the size of the small LF-NPs was again in good agreement with that of the initial OA-capped NaLuF<sub>4</sub> NPs, indicating a certain resistance of the sample to phase transformation. Moreover, the ribbon-like structures shown in Figure S9 and S10A-3 have been described by Becerro *et al.* as a possible morphology adopted by orthorhombic LuF<sub>3</sub> as reported.<sup>7</sup>

## 7. RE<sup>3+</sup> Ion Dependence – $\beta$ -NaREF<sub>4</sub> as Starting NPs

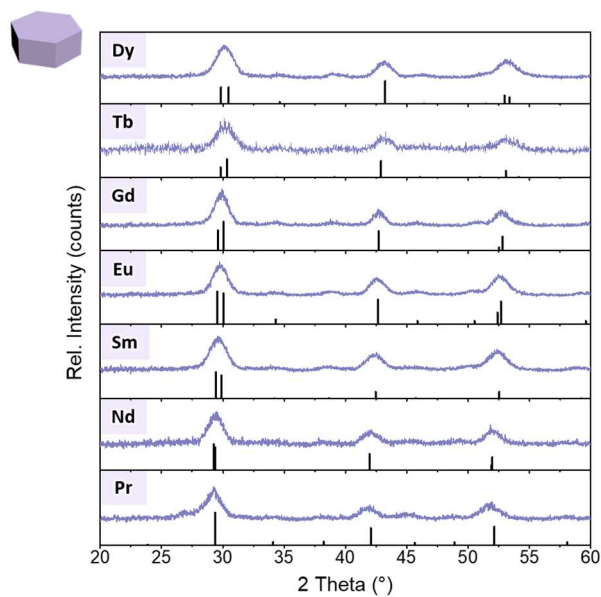


**Figure S11:** XRD patterns of  $\beta$ -NaREF<sub>4</sub> NPs obtained by microwave-assisted thermal decomposition. RE refers to the rare earth ions studied as labelled for each pattern. References:  $\beta$ -NaPrF<sub>4</sub>, PDF card [01-082-4240];  $\beta$ -NaNdF<sub>4</sub>, PDF card [00-027-0756];  $\beta$ -NaSmF<sub>4</sub>, PDF card [00-027-0779];  $\beta$ -NaEuF<sub>4</sub>, PDF card [00-028-1085];  $\beta$ -NaGdF<sub>4</sub>, PDF card [01-080-8787];  $\beta$ -NaTbF<sub>4</sub>, PDF card [00-027-0809];  $\beta$ -NaDyF<sub>4</sub>, PDF card [00-027-0687].

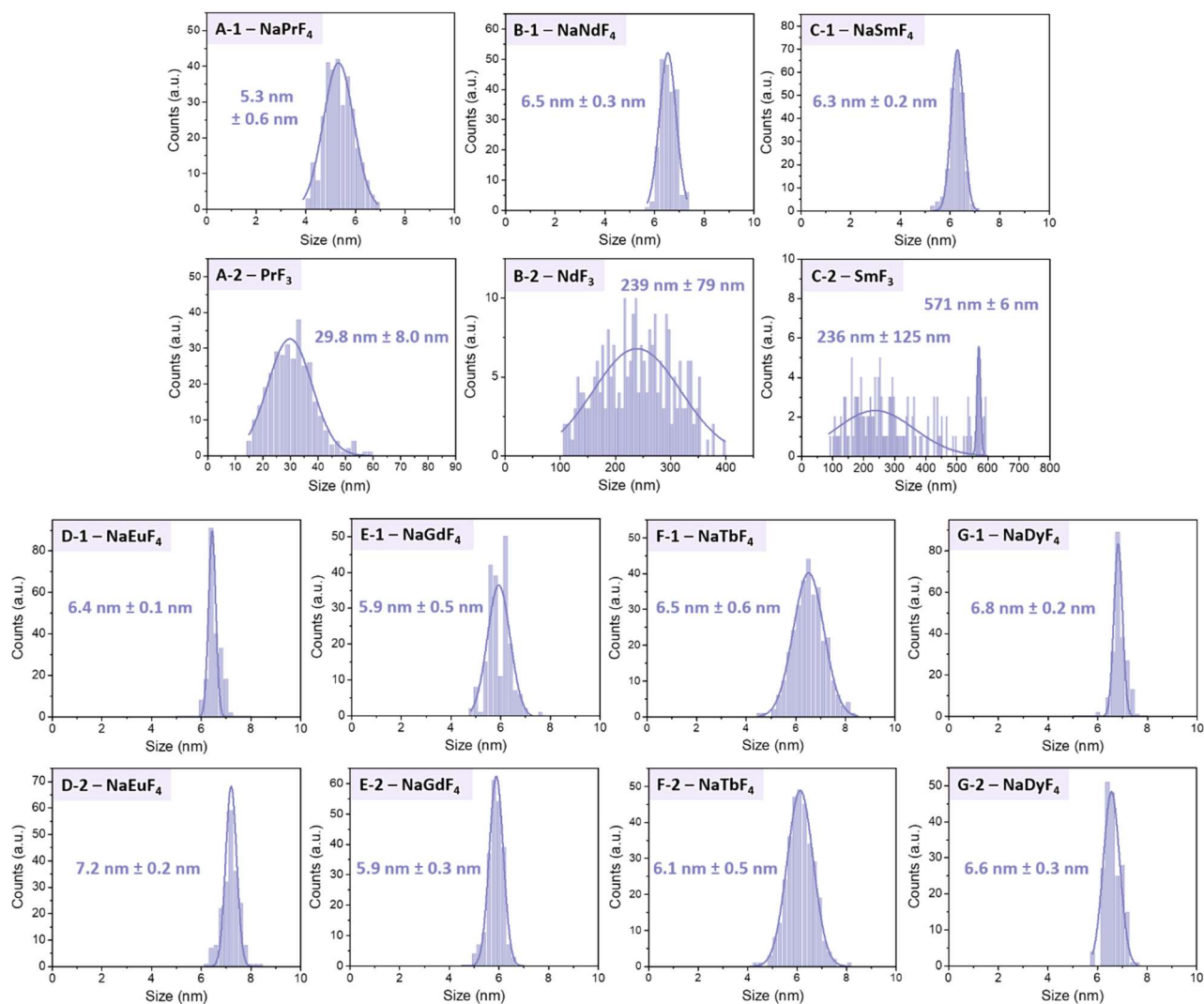


**Figure S12:** Average particle sizes and size distributions of (1) OA-capped  $\beta$ -NaREF<sub>4</sub> NPs obtained by microwave-assisted thermal decomposition and (2) their respective ligand-free counterparts obtained by stirring at pH 1.5 for 20 h. RE = (A) Pr, (B) Nd, (C) Sm, (D) Eu, (E) Gd, (F) Tb, and (G) Dy.

## 8. Influence of Ln<sup>3+</sup>-Doping on the Formation of GdF<sub>3</sub> from $\alpha/\beta$ -NaGdF<sub>4</sub>

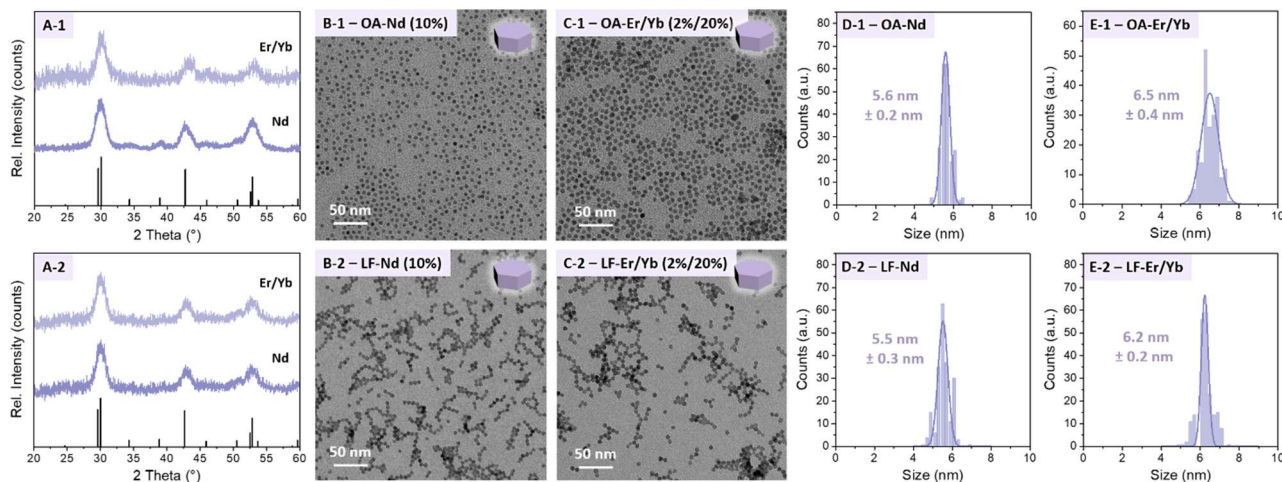


**Figure S13:** XRD patterns of (A-1) OA-capped and (A-2) ligand-free  $\beta$ -NaGdF<sub>4</sub> NPs doped with 10% Nd<sup>3+</sup> and 2%/20% Er<sup>3+</sup>/Yb<sup>3+</sup>, respectively. References:  $\beta$ -NaGdF<sub>4</sub>, PDF card [01-080-8787]. TEM images of (1) OA-capped and (2) ligand-free  $\beta$ -NaGdF<sub>4</sub> NPs doped with (B) 10% Nd<sup>3+</sup>, and (C) 2%/20% Er<sup>3+</sup>/Yb<sup>3+</sup>, respectively. All LF-NPs were obtained by stirring at pH 1.5 for 20 h. The respective average sizes and size distributions are shown in (D) and (E).

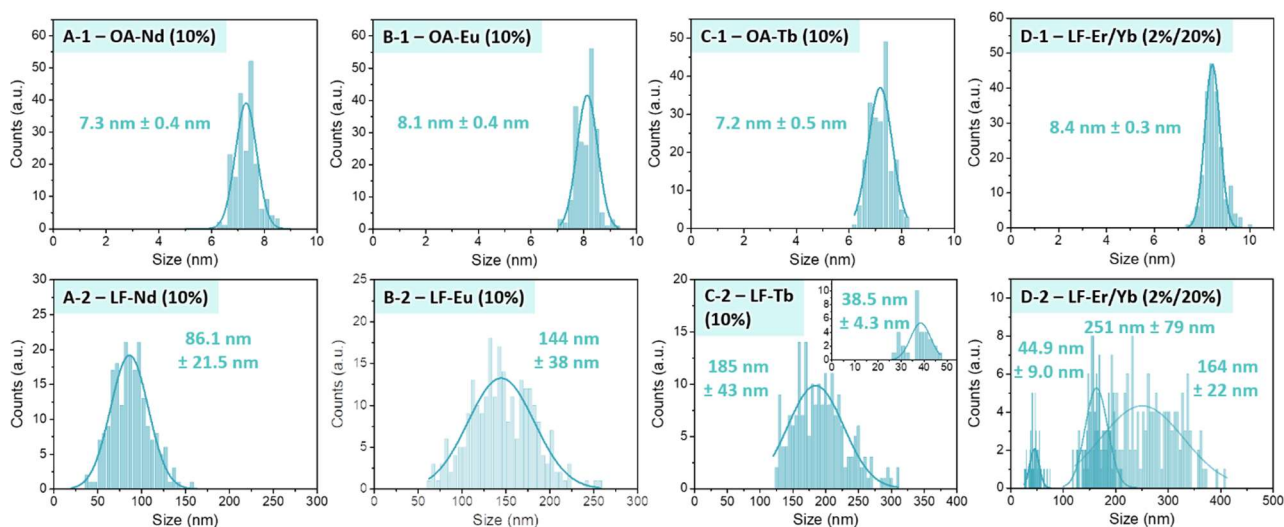


**Figure S14:** Average sizes and size distributions of (1) OA-capped Ln<sup>3+</sup>-doped  $\alpha$ -NaGdF<sub>4</sub> NPs used for ligand removal (pH 1.5, 20 h) yielding Ln<sup>3+</sup>-doped GdF<sub>3</sub> particles shown in Figures 7 and S15. (2) Sizes and size distributions of ligand-free NPs. Ln = (A) Nd (10%), (B) Eu (10%), (C) Tb (10%), and (D) Er/Yb (2%, 20%), respectively. The inset in (C-2) provides an estimated value for the thickness of the obtained plates. Dimensions given in (D-2) correspond to the thickness, width and length of the Er<sup>3+</sup>/Yb<sup>3+</sup>-doped GdF<sub>3</sub> bundles.

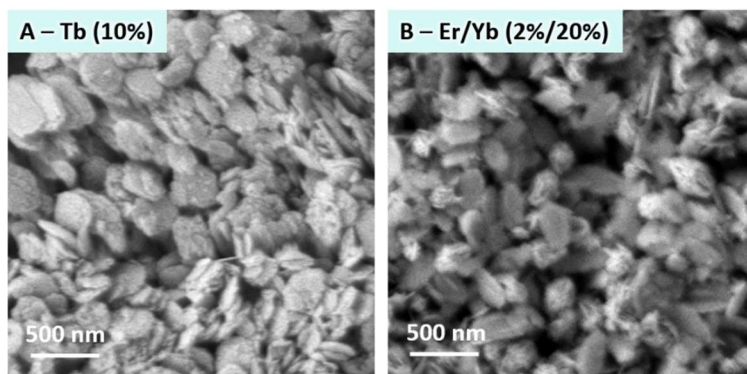


**Figure S15:** SEM images of ligand-free (A) hexagonal  $\text{GdF}_3$  doped with 10%  $\text{Tb}^{3+}$  and (B) orthorhombic  $\text{GdF}_3$  co-doped with 2%  $\text{Er}^{3+}$  and 20%  $\text{Yb}^{3+}$ . Both samples were obtained upon stirring of the respective  $\text{Ln}^{3+}$ -doped  $\alpha\text{-NaGdF}_4$  NPs at pH 1.5 for 20 h.

## 9. Steady State and Time-Resolved Spectroscopy of Ln<sup>3+</sup>-Doped $\alpha/\beta$ -NaGdF<sub>4</sub> and GdF<sub>3</sub>

**Table S6:** Overview of NP concentrations, excitation wavelength ( $\lambda_{EX}$ ), and power of the excitation source used for steady state and time-resolved spectroscopy of OA-capped and ligand-free (LF) Ln<sup>3+</sup>-doped NaGdF<sub>4</sub> and GdF<sub>3</sub> NPs.

Ln <sup>3+</sup> Dopant	NaGdF <sub>4</sub> Crystalline Phase	OA-NP Concentration (mg/mL)	LF-NP Crystalline Phase <sup>a</sup>	LF-NP Concentration (mg/mL)	$\lambda_{EX}$ (nm)	Power OA / LF <sup>b</sup> (W)
Nd (10%)	$\alpha$	33	h-GdF <sub>3</sub>	13	808	1.30
	$\beta$	15	$\beta$ -NaGdF <sub>4</sub>	3		
Eu (10%)	$\alpha$	42	h-GdF <sub>3</sub>	18	394	75 <sup>c</sup>
Tb (10%)	$\alpha$	54	h-GdF <sub>3</sub>	11	311	75 <sup>c</sup>
Er/Yb (2%/20%)	$\alpha$	5	o-GdF <sub>3</sub>	5	980	1.35 / 1.83
	$\beta$	2	$\beta$ -NaGdF <sub>4</sub>	6		

<sup>a</sup> h = hexagonal, o = orthorhombic

<sup>b</sup> The same laser power was used for OA-capped and LF-NPs, unless stated otherwise.

<sup>c</sup> 75 W Xenon lamp

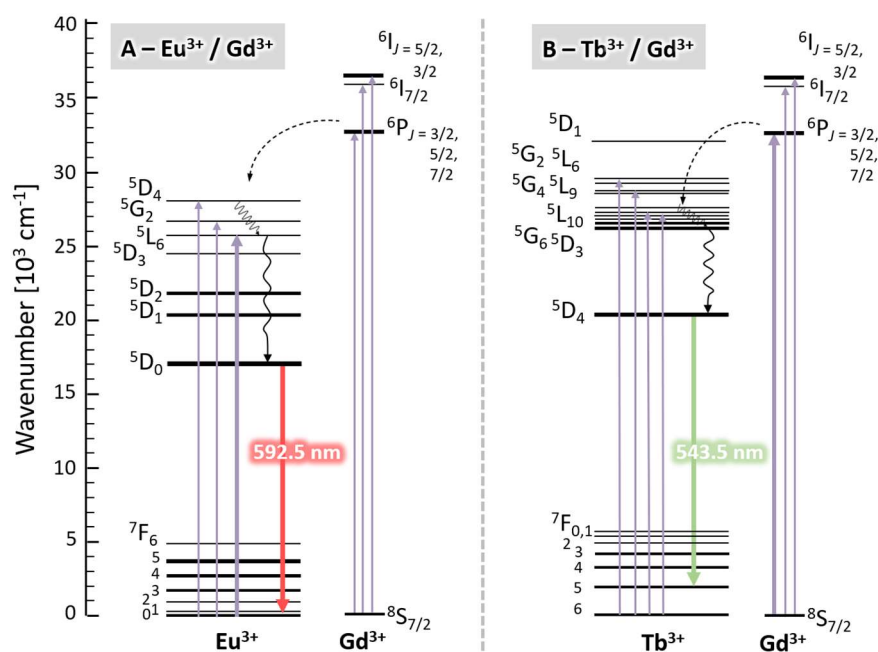


**Figure S16:** Energy level schemes for (A) the Eu<sup>3+</sup>/Gd<sup>3+</sup> and (B) the Tb<sup>3+</sup>/Gd<sup>3+</sup> pair showing the respective f-f transitions observed at the excitation spectra given in Figure 8A/B.

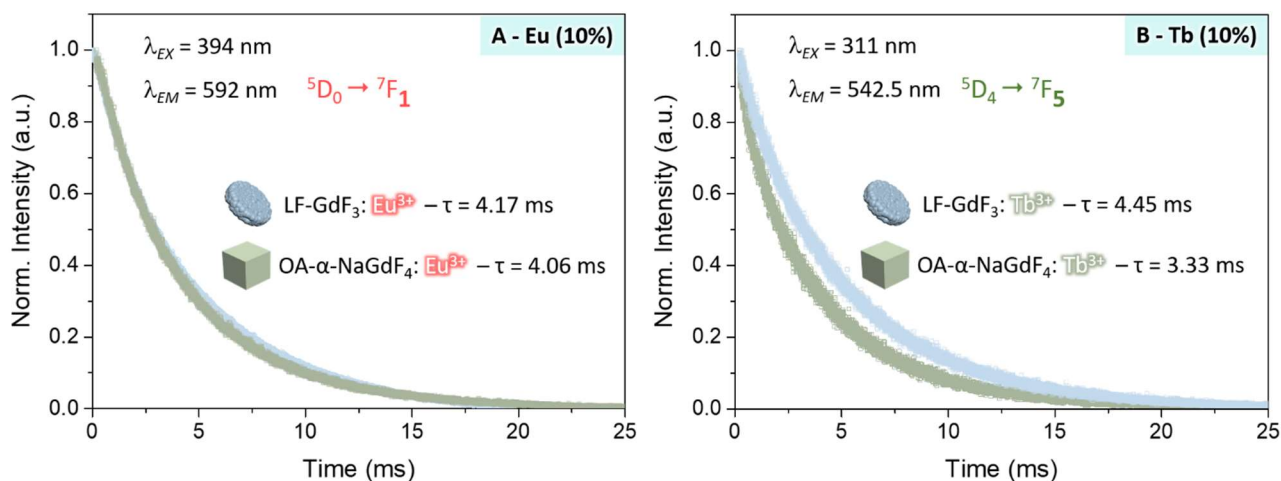


**Figure S17:** Fluorescence decay curves and respective lifetime values for the indicated transitions of samples doped with (A)  $\text{Eu}^{3+}$  (10%), (B)  $\text{Tb}^{3+}$  (10%).

**Lifetime measurements.** The lifetime values given in Figure S17 (and S19 – *vide infra*) were obtained by integration of the area under the respective decay curves. In case of  $\text{Nd}^{3+}$ -doped samples (Figure S19), the instrument response function (IRF) is plotted together with the lifetime decay curves. The lifetimes of these samples were obtained in a region not being influenced by the IRF.

**Lifetimes of UV-excited emissions ( $\text{Eu}^{3+}$ ,  $\text{Tb}^{3+}$ ).** Interestingly, in case of the  $\text{Eu}^{3+}$ -doped samples, the phase transformation from  $\alpha\text{-NaGdF}_4$  to hexagonal  $\text{GdF}_3$  did not result in any major change of the lifetime of the  $\text{Eu}^{3+}$   ${}^5\text{D}_0 \rightarrow {}^7\text{F}_2$  emission (Figure 17A). This speaks for the fact that, despite the significant size increase upon  $\alpha\text{-NaGdF}_4$ -to- $\text{GdF}_3$  phase transformation from 8.1 to 144 nm, the non-radiative processes in both samples must be very similar.  $\text{Tb}^{3+}$ -doped NPs underwent a similar size increase upon phase transformation from 7.2 to 185 nm. Herein, as expected, the increase in NP size came along with a longer lifetime, indicating that the phase transformation partially suppressed non-radiative decay pathways for the  $\text{Tb}^{3+}$   ${}^5\text{D}_4 \rightarrow {}^7\text{F}_6$  emission (Figure 17B).

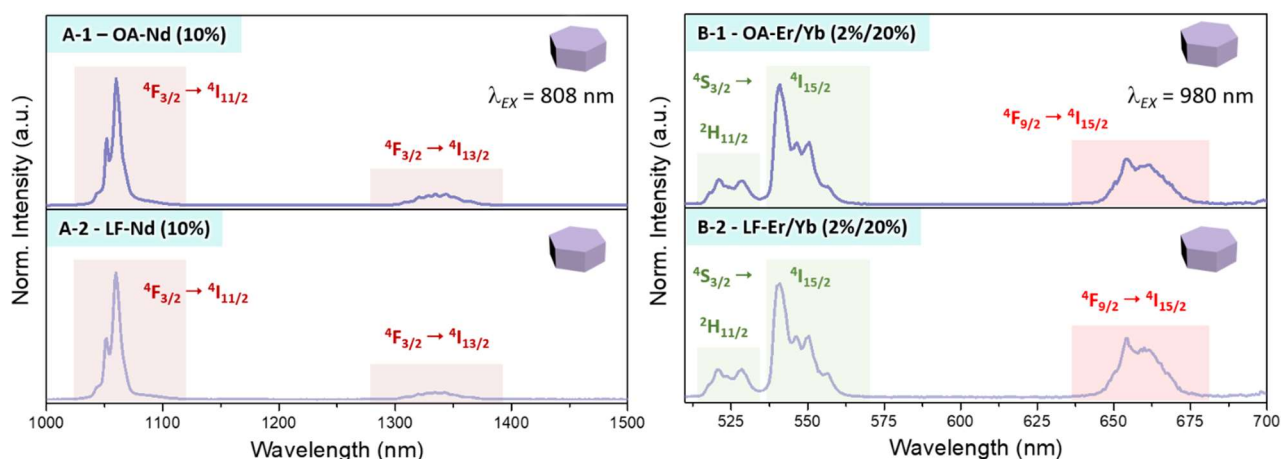


**Figure S18:** NIR emission spectra for (A-1) OA-capped and (A-2) ligand-free  $\text{Nd}^{3+}$ -doped  $\beta\text{-NaGdF}_4$  as well as upconversion emission spectra for (B-1) OA-capped and (B-2) ligand-free  $\text{Er}^{3+}/\text{Yb}^{3+}$ -doped  $\beta\text{-NaGdF}_4$ .

**NIR-excited NIR and UC emission ( $\text{Nd}^{3+}$ ,  $\text{Er}^{3+}/\text{Yb}^{3+}$ ).** Emission spectra shown in Figure S18 correspond to the hexagonal-phase  $\text{Ln}^{3+}$ -doped samples that, as discussed in the main text, did not undergo any phase transformation to  $\text{GdF}_3$  upon acidic treatment. It is evident from these emission spectra, exhibiting the

characteristic  $\text{Nd}^{3+}$  (Figure 18A) and  $\text{Er}^{3+}$  (Figure 18B) emission peaks, that the spectral profiles of the samples did not change significantly upon transfer from the organic into the aqueous phase.

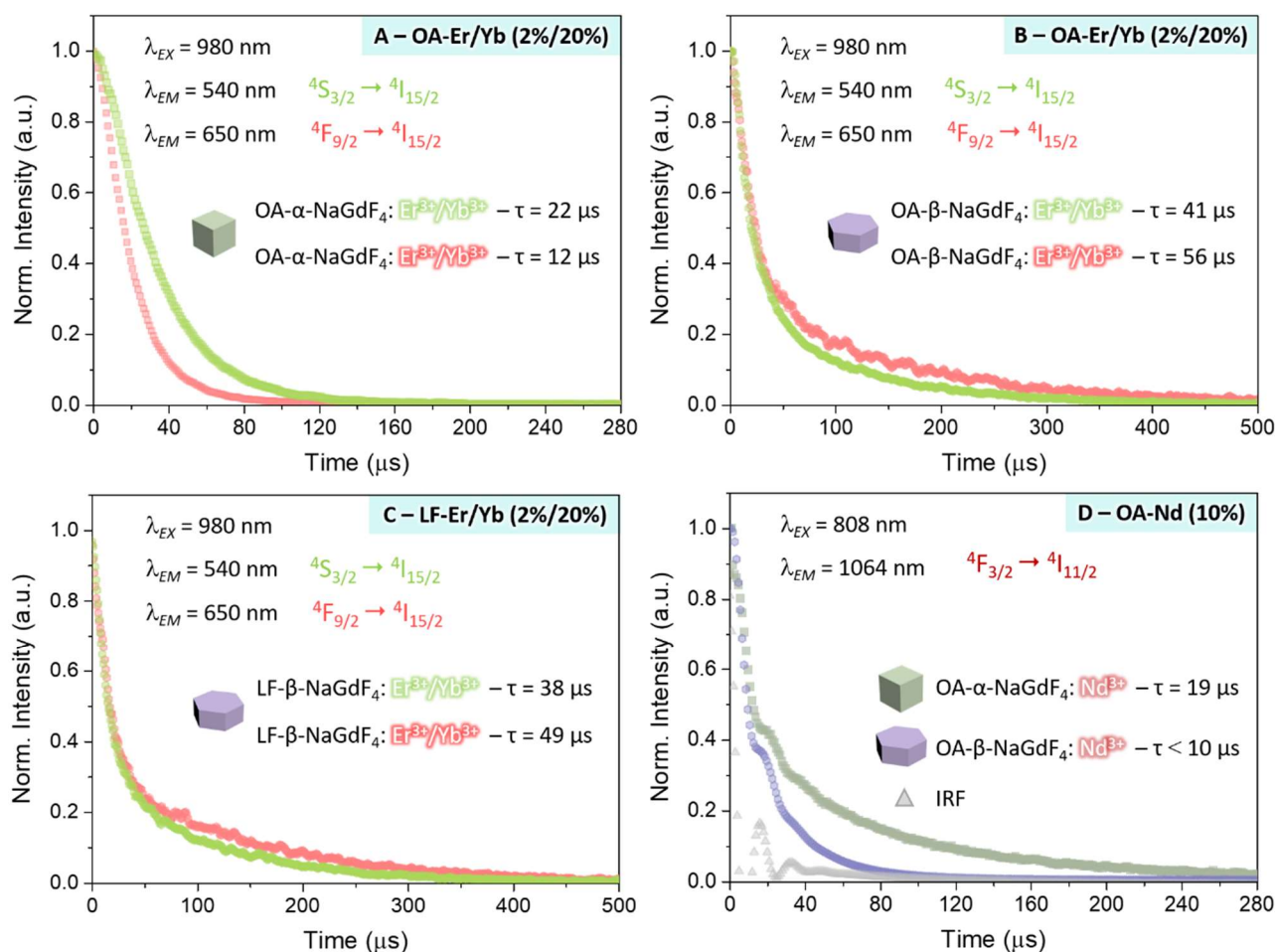


**Figure S19:** Fluorescence decay curves and respective lifetime values for the indicated transitions of (A) OA-capped  $\alpha$ - $\text{NaGdF}_4$  doped with  $\text{Er}^{3+}/\text{Yb}^{3+}$  (2%/20%), (B) and (C) OA-capped and ligand-free (LF)  $\beta$ - $\text{NaGdF}_4$  doped with  $\text{Er}^{3+}/\text{Yb}^{3+}$  (2%/20%), and (D)  $\alpha$ - and  $\beta$ - $\text{NaGdF}_4$  doped with  $\text{Nd}^{3+}$  (10%). IRF: instrument response function of the InGaAs detector.

**Lifetimes of NIR-excited emissions ( $\text{Er}^{3+}/\text{Yb}^{3+}$ ,  $\text{Nd}^{3+}$ ).** For OA-capped  $\text{Er}^{3+}/\text{Yb}^{3+}$ -doped  $\alpha$ - and  $\beta$ - $\text{NaGdF}_4$  NPs, lifetimes of both the green ( $^4\text{S}_{3/2} \rightarrow ^4\text{I}_{15/2}$ ) and the red ( $^4\text{F}_{9/2} \rightarrow ^4\text{I}_{15/2}$ ) emission were found to be in a similar range as previously reported, namely around 50  $\mu\text{s}$  (Figure S19A/B/C).<sup>1</sup> Not surprisingly, lifetime shortening was observed for ligand-free  $\text{Er}^{3+}/\text{Yb}^{3+}$ -doped  $\beta$ - $\text{NaGdF}_4$  NPs when compared to their OA-capped counterparts (Figure S19C), indicating stronger contribution of non-radiative processes, *e.g.* due to interaction with the solvent, *i.e.* water. As discussed in the main manuscript, the  $\alpha$ - $\text{NaGdF}_4$ -to- $\text{GdF}_3$  phase transformation resulted in orthorhombic ligand-free  $\text{Er}^{3+}/\text{Yb}^{3+}$ -doped  $\text{GdF}_3$  NPs. Their weak upconversion emission intensity did not allow to obtain an emission decay curve for this sample.

Relatively short lifetimes were determined for the  $^4\text{F}_{3/2} \rightarrow ^4\text{I}_{11/2}$  NIR emission of  $\text{Nd}^{3+}$ -doped OA-capped  $\alpha$ - and  $\beta$ - $\text{NaGdF}_4$  NPs; namely 19  $\mu\text{s}$  for the  $\alpha$ -NPs, while even shorter values of less than 10  $\mu\text{s}$  were estimated for the  $\beta$ -NPs (Figure 19D). Such short lifetimes may be ascribed to the relatively high  $\text{Nd}^{3+}$  dopant concentration of 10%: it is known that higher concentrations foster cross-relaxation processes, which can result in shorter lifetime values.<sup>8</sup> In addition to dopant concentration optimization, the use of sensitizer/activator pairs and application of the core/shell concept to avoid surface-related quenching processes are suitable strategies

towards NPs of longer lifetimes. For instance, Ce/Nd-co-doped NaGdF<sub>4</sub> core/shell architectures (5% Nd<sup>3+</sup>) were reported to exhibit a one order of magnitude longer lifetime (150 μs) than our sub-10 nm core-only NPs.<sup>9</sup> Yet, it should be kept in mind that our work focuses on aspects of materials chemistry, rather than optimization of the NPs' optical performance. The corresponding ligand-free Nd<sup>3+</sup>-doped β-NaGdF<sub>4</sub> NPs exhibited too weak emission when dispersed in water, not allowing for reliable lifetime measurements.

Table S7 summarizes the results obtained by time-resolved spectroscopy.

**Table S7:** Overview all obtained lifetime values.

Ln <sup>3+</sup> Dopant	Monitored Transition	NaGdF <sub>4</sub> Crystalline Phase	GdF <sub>3</sub> Crystalline Phase	Lifetime	
				OA-NPs	LF-NPs
Eu (10%)	<sup>5</sup> D <sub>0</sub> → <sup>7</sup> F <sub>1</sub>	α		4.06 ms	
			hexagonal		4.17 ms
Tb (10%)	<sup>5</sup> D <sub>4</sub> → <sup>7</sup> F <sub>5</sub>	α		3.33 ms	
			hexagonal		4.45 ms
Er/Yb (2%/20%)	<sup>4</sup> S <sub>3/2</sub> → <sup>4</sup> I <sub>15/2</sub>	α		22 μs	
			orthorhombic		– <sup>a</sup>
		β		41 μs	38 μs
	<sup>4</sup> F <sub>9/2</sub> → <sup>4</sup> I <sub>15/2</sub>	α		12 μs	
		orthorhombic		– <sup>a</sup>	
Nd (10%)	<sup>4</sup> F <sub>3/2</sub> → <sup>4</sup> I <sub>11/2</sub>	α	hexagonal	19 μs	– <sup>a</sup>
		β		< 10 μs <sup>b</sup>	– <sup>a</sup>

<sup>a</sup> Emission intensity too weak.

<sup>b</sup> Based on the experimentally determined decay curve and the instrument response function (IRF), a lifetime of *ca.* 4 μs was obtained, yet, such short value must be taken with care due to instrumental limitations.

## 10. References

1. I. Halimi, E. M. Rodrigues, S. L. Maurizio, H.-Q. T. Sun, M. Grewal, E. M. Boase, N. Liu, R. Marin and E. Hemmer, *J. Mater. Chem. C*, 2019, **7**, 15364-15374.
2. L. Zhang, R. He and H.-C. Gu, *Appl. Surf. Sci.*, 2006, **253**, 2611-2617.
3. N. Bogdan, F. Vetrone, G. A. Ozin and J. A. Capobianco, *Nano Lett.*, 2011, **11**, 835-840.
4. Y. Gu, X. Qiao, J. Zhang, Y. Sun, Y. Tao and S. Qiao, *Chem. Res. Chin. Univ.*, 2016, **32**, 474-479.
5. E. Hemmer, M. Quintanilla, F. Légaré and F. Vetrone, *Chem. Mater.*, 2014, **27**, 235-244.
6. A. Lay, O. H. Sheppard, C. Siefe, C. A. McLellan, R. D. Mehlenbacher, S. Fischer, M. B. Goodman and J. A. Dionne, *ACS Cent. Sci.*, 2019, **5**, 1211-1222.
7. A. I. Becerro, D. Gonzalez-Mancebo and M. Ocaña, *J. Nanopart. Res.*, 2015, **17**, 58.
8. J. Bergstrand, Q. Liu, B. Huang, X. Peng, C. Wurth, U. Resch-Genger, Q. Zhan, J. Widengren, H. Agren and H. Liu, *Nanoscale*, 2019, **11**, 4959-4969.
9. T. Sun, X. Chen, L. Jin, H. W. Li, B. Chen, B. Fan, B. Moine, X. Qiao, X. Fan, S. W. Tsang, S. F. Yu and F. Wang, *J. Phys. Chem. Lett.*, 2017, **8**, 5099-5104.